HHS Public Access

Author manuscript

Anal Chem. Author manuscript; available in PMC 2018 February 07.

Published in final edited form as:

Anal Chem. 2017 February 07; 89(3): 1516–1522. doi:10.1021/acs.analchem.6b03353.

Structural characterization of phosphatidylcholines using 193 nm ultraviolet photodissociation mass spectrometry

Dustin R. Klein and **Jennifer S. Brodbelt**

Department of Chemistry, The University of Texas at Austin, Austin, TX 78712

Abstract

Advances in mass spectrometry have made it a preferred tool for structural characterization of glycerophospholipids. Collisional activation methods commonly implemented on commercial instruments do not provide fragmentation patterns that allow elucidation of certain structural features, including acyl chain positions on the glycerol backbone and double bond positions within acyl chains. In the present work, 193 nm ultraviolet photodissociation (UVPD) implemented on an Orbitrap mass spectrometer is used to localize double bond positions within phosphatidylcholine (PC) acyl chains. Cleavage of the carbon-carbon bonds adjacent to the double bond provides a diagnostic mass difference of 24 Da and enables differentiation of double-bond positional isomers. The UVPD method was extended to the characterization of PCs in a bovine liver extract via a shotgun strategy. Positive mode higher energy collisional dissociation (HCD) and UVPD, and negative mode HCD were undertaken in a complementary manner to identify species as PCs and to localize double bonds, respectively.

TOC Image

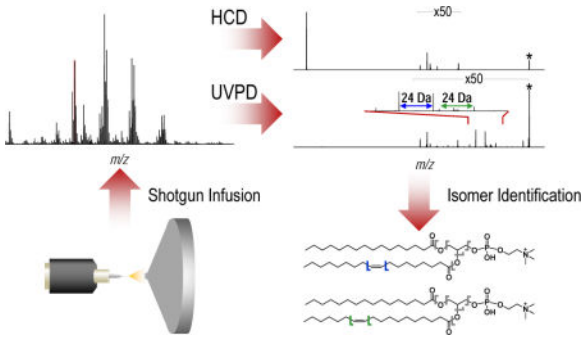

Correspondence to: jbrodbelt@cm.utexas.edu.

Supporting Information: Addition figures and tables include the structures, masses and full mass spectra of all standard phosphatidylcholines (PCs), HCD and UVPD spectra of Na-cationized PC 16:0/18:1(9Z), HCD and UVPD spectra for PC 16:0/18:0, PC 16:0/18:1(9Z), PC 18:1(9Z)/16:0, and PC 16:0/18:1(9Z, 12Z), HCD and UVPD spectra for all PCs identified in the polar bovine liver extract, full mass spectra and zoomed in UVPD mass spectra of samples containing varying molar ratios of PC 18:1(9Z)/18:1(9Z) and PC 18:1(6Z)/18:1(6Z). All figures with HCD and UVPD spectra contain accompanying fragmentation maps. This material is available free of charge via the Internet at http://pubs.acs.org.

Introduction

Glycerophospholipids, a diverse subclass of lipids and the main component of cell membranes, have been the focus of many targeted lipidomics studies. In addition to heavily influencing cell membrane dynamics, they also participate in cellular signaling and can influence the organization and structure of proteins within the membrane. [1–5] Despite their relatively low molecular weights compared to other biomolecules, glycerophospholipids are highly complex as a result of the various combinations of substituents that can occur at each of the three positions of the glycerol backbone.[6–8] Consequently, glycerophospholipid isomers are commonplace, with subtle differences potentially having large implications for biological function.[1,3,9–12] Considering the impact of specific structural features on membrane dynamics, a detailed characterization of glycerophospholipids is necessary to achieve a full understanding of cellular behavior. Two general mass spectrometric approaches to analyze lipids have been developed: one employing separations with either liquid chromatographic (LC) mass spectrometry[13] or ion mobility methods[14–16], and the other based on direct infusion of lipids extracts, the latter termed “shotgun lipidomics”[17–23] With both of these approaches mass spectrometric data can be collected in either a top-down or bottom-up fashion. [1,23] In lipidomics, top-down methods rely on high resolution MS data to accurately determine lipid molecular formulae, whereas bottom-up methods utilize MS/MS spectra to identify a specific lipid or class of lipids.[22,23]

Collection of mass spectrometric data in a top-down fashion for glycerophospholipid analysis, using either LC or a shotgun approach, is high throughput, gives a global profile of lipid composition, and can differentiate isobars at high resolution, yet it provides no structural information and therefore does not permit differentiation of isomers.[22] Advances in tandem mass spectrometry have allowed significant inroads into the structural analysis of glycerophospholipids. The most commonly employed and well-studied method of fragmentation for bottom-up lipid analysis is collision induced dissociation (CID). Fragmentation patterns in positive and negative mode produce predominant fragments corresponding to the head group and acyl chains, respectively.[17,24] The different ionization efficiencies of glycerophospholipid subspecies can often dictate the mode of analysis. In an attempt to improve ionization efficiencies, methods involving chemical modification of glycerophospholipid head groups have been developed. Specifically, Wasslen *et al.* and Canez *et al.* trimethylated the glycerophospholipid amino groups to improve ionization in positive mode.[25,26] Methods that utilize polarity switching have also been developed.[22] However, the mode in which ionization is optimal may not produce MS/MS spectra containing the desired structural information. Ion-ion reactions and ion adduction have thus been used to overcome these obstacles.[27–29] Stutzman *et al.* reacted phosphatidylcholine cations with doubly deprotonated 1,4-phenylenedipropionic acid in the gas phase to produce phosphatidylcholine anions that, upon CID fragmentation, produced informative fragmentation patterns with enhanced signal-to-noise.[27] In addition, Ho *et al.* found that CID of glycerophospholipid-metal cation complexes gave more informative spectra.[29]

Conventional CID methods provide structural information regarding the acyl chain lengths, number of unsaturated C-C bonds, and head groups; however, often CID does not reveal some of the more subtle structural characteristics of glycerophospholipids, including acyl

chain position and double bond position. Therefore, the development of new analytical tools to completely characterize glycerophospholipid structures and quantify their abundances remains an active area of interest. For example, Hsu and Turk used lithium adduction and an MS^n approach to determine double bond position.[30] Xia and coworkers recently reported a selective reaction/CID strategy to elucidate the position of double bonds in the acyl chains and quantify the relative abundances of mixtures of double bond isomers.[31–33] The key step exploited the well-known Paternò-Bücci reaction which causes photochemical formation of an oxetane ring from a ketone/aldehyde and double bonds within the acyl chains.[31–33] Yang *et al.* employed a strategy in which the variation in abundances of neutral loss products were monitored as a function of double bond position to identify both the double bond position and quantify relative amounts of fatty acid isomers.[34] Additional methods have focused on novel ion activation techniques including radical-directed dissociation (RDD) via 266 nm photodissociation followed by CID[35–37], ozone induced dissociation (OzID)[38–40], electronic impact excitation of ions from organics (EIEIO)[41], metastable atom-activated dissociation (MAD)[42,43] and electron transfer dissociation (ETD)[44]. In parallel studies Pham *et al.* explored non-covalent complexation of 4-iodobenzoic acid, 4-iodoaniline or 4-iodobenzoyl 18-crown-6 to glycerophospholipids and reactions of 4-iodobenzyl alcohol with fatty acids.[35–37] Irradiation with 266 nm photons resulted in radical species that allowed assignment of double bond position upon CID.[35–37] OzID involves the gas-phase reaction of isolated glycerophospholipid cations with ozone in an ion trap[39,40]; CID subsequently provided information regarding double bond positions and *sn*-position. While EIEIO, MAD and ETD are each initiated by reactions of ions with electrons, metastable helium or argon atoms, or radical anions, respectively, these methods appear to induce similar radical-based fragmentation pathways.

Another ion activation method that produces rich fragmentation spectra for various biomolecules, including lipids, is 193 nm ultraviolet photodissociation (UVPD).[45–51] Absorption of a 193 nm photon results in deposition of ~6.4 eV of internal energy, and the photoactivation process occurs in a 5 ns laser pulse period. This higher energy excitation affords access to fragmentation pathways not observed by collision based methods, ultimately providing richer fragmentation patterns that have been useful for characterizing lipooligosaccharides[49,52]and gangliosides,[47] as well as other types of biological molecules.[45] In the present study, 193 nm (UVPD) is shown to produce fragmentation patterns that allow double-bond isomer differentiation and is used for detailed structural characterization of mixtures of phosphatidylcholines (PCs), a subclass of glycerophospholipids highly abundant in mammalian cells.[5]

Experimental

All PC samples as well as the polar bovine liver extract were purchased from Avanti Polar Lipids (Alabaster, Alabama) and were used without further purification. The structures and molecular weights of all PCs included in the study are shown in Table S1. Lipid shorthand notation used is in accordance with previously established notation.[53] In brief, acyl chain compositions are indicated by the number of carbons atoms in the acyl chain followed by a colon and the number double bonds. For PCs with known acyl chain orientation, the acyl chain compositions of *sn-1* and *sn-2* are separated by "/" with *sn*-1 followed by *sn-2*. For

unknown acyl chain orientation, acyl chain compositions are separated by "_". For known double bond positions, positions are indicated in parenthesis after the acyl chain composition by the carbon number and Z, E or Δ to indicate the bond orientation as *cis, trans* or unknown, respectively. For example, PC 16:0/18:1(9Z) represents a phosphatidylcholine with palmitate (16 carbon chain) at the *sn*-1 position and oleate (18 carbon chain with 1 unsaturation) at the *sn*-2 position with a *cis* double bond at carbon number 9. Methanol (MeOH), acetonitrile (ACN) and water were purchased from EMD Millipore (Billerica, MA), HPLC grade chloroform and LC-MS grade ammonium formate were purchased from Sigma Aldrich (St. Louis, MO). All samples were diluted in 50:50 acetonitrile:water with 30 mM ammonium formate to 10 μM for PC standards and 10 μg/mL for polar bovine liver extract unless otherwise indicated. Approximately 10 μL of sample were loaded into a silver-coated pulled tip glass capillary (1.2 mm OD) and sprayed using a Proxeon offline nano-electrospray set-up (Thermo Scientific, San Jose, CA). The spray voltage was set to 1.1 kV. All positive mode spectra were collected on either a Thermo Scientific Orbitrap Fusion Lumos or Orbitrap Elite mass spectrometer (San Jose, CA) modified with a 193 nm Coherent Existar excimer laser (Santa Cruz, CA) to perform UVPD as previously described.[51,52] On the Orbitrap Elite mass spectrometer, UVPD was performed in the HCD cell with 8 laser pulses at 5 mJ per pulse, and on the Orbitrap Fusion Lumos mass spectrometer, UVPD was performed in the low pressure trap of the dual linear ion trap by applying 10 laser pulses at 6 mJ per pulse. In each case, the laser was operated at 500 Hz, resulting in an activation period of 16 to 20 ms per scan. For UVPD-CID spectra collected on the Orbitrap Fusion Lumos mass spectrometer, UVPD activation was first performed in the high pressure trap of the dual linear ion trap with 10 laser pulses at 6 mJ per pulse followed by CID with a normalized collision energy (NCE) of 30. All negative ion mode spectra were collected on the Thermo Scientific Orbitrap Fusion Lumos mass spectrometer. Data were collected with an AGC target between 5×10^4 and 1×10^5 at a resolution of 60,000. To maximize the quality of the benchmark MS/MS spectra, 100 scans were averaged with 2 μscans per scan, corresponding to approximately one minute per spectrum. MS/MS spectra could be collected with as few as one scan per spectrum, as shown in Figure S1. All HCD data were collected with an NCE of 25. On the Orbitrap Fusion Lumos mass spectrometer an isolation width of 1 Da was used and on the Orbitrap Elite mass spectrometer an isolation width of 2 was used. Default activation times were used for HCD. All data were analyzed in XCalibur Qual Browser and manually interpreted.

Results and Discussion

For this study, a series of PCs were characterized by HCD and UVPD in order to compare the types of fragment ions produced by each activation and evaluate the capability for localization of double bonds and isomer/isobar differentiation. Infusion of each PC in positive mode yielded abundant protonated ($[M+H]^+$) and less abundant sodium cationized ($[M+Na]^+$) ions (Figure S2). Examples of the HCD and UVPD mass spectra are shown in Figures 1 and 2. As an example, higher energy collisional dissociation (HCD) of protonated PC 16:0/18:1(9Z) produced an abundant product ion of *m/z* 184.07, corresponding to the phosphocholine head group, and less abundant ions of *m/z* 478.33, 496.34, 504.35 and 522.35 corresponding to acyl chain neutral losses (Figure 1a). All ions observed upon HCD

are consistent with results previously reported for collisional activation of PCs.[54] UVPD produced the same acyl chain neutral loss ions as well as highly informative ions corresponding to C-C cleavages along the acyl chain. The UVPD mass spectrum lacks the predominant headgroup ion of *m/z* 184 as a result of the default ion trap q-value when performing UVPD on the Orbitrap Fusion Lumos mass spectrometer; with the current software, the ion trap q-value cannot be decreased below a default value of 0.25. To confirm that the headgroup ion is in fact generated upon UVPD, HCD and UVPD spectra were collected on an Orbitrap Elite mass spectrometer also equipped with a 193 nm excimer laser, with UVPD performed in the HCD cell (Figure S3). The UVPD mass spectrum collected on the Orbitrap Elite mass spectrometer confirms that the headgroup ion of *m/z* 184 is generated. The most abundant of the C-C acyl chain cleavage products (*m/z* 622.45 and *m/z* 646.45) correspond to cleavage of either one of the carbon-carbon bonds adjacent to the double bond. The 24 Da mass difference allows facile recognition of this diagnostic pair of ions. Putative structures of the two marker ions are shown in Figure S4. This pair of key diagnostic ions is also generated upon UVPD of the corresponding sodium-cationized PC, as illustrated in Figure S5. HCD of sodium-cationized PC 16:0/18:1(9Z) results predominantly in neutral losses of choline and phosphocholine (yielding the products of *m/z* 723.49 and *m/z* 599.50, respectively), again providing characteristic head group information. Additionally, acyl chain neutral losses consistent with retention or loss of sodium are also observed. In the corresponding UVPD mass spectrum, fragment ions produced by cleavage of the carbon-carbon bond on either side of the double bond are again observed (*m/z* 644.43 and 668.43). Both of these ions retain sodium and confirm that UVPD of sodium-adducted species provides the same type of double bond positional information as noted for the protonated PC. For the remainder of the study, the analysis will focus on the protonated PCs.

HCD and UVPD spectra of the isomeric lipids PC 18:1(9Z)/18:1(9Z) and PC 18:1(6Z)/18:1(6Z) are shown in Figure 2. The HCD spectra display informative head group (*m/z* 184.07) and diagnostic acyl chain (*m/z* 504.34 and 522.36) ions, but the HCD spectra for these isomeric PCs are indistinguishable. In contrast, the fragmentation patterns generated by UVPD exhibit ions that allow differentiation of the double bond positional isomers based on the unique C-C cleavage products that differ by 24 Da. The most abundant C-C cleavage fragments for PC 18:1(9Z)/18:1(9Z) are *m/z* 648.46 and 672.46, and for PC 18:1(6Z)/18:1(6Z) they are *m/z* 606.41 and 630.41. In addition, the UVPD spectra of PC 16:0/18:1(9Z), PC 18:1(9Z):18:1(9Z), PC 18:1(6Z)/18:1(6Z) and all other PCs with double bonds exhibit the loss of a hydrogen atom from the precursor, resulting in products of *m/z* 759.57, *m/z* 785.57 and *m/z* 785.57, respectively, and also display other odd-electron fragment ions that are suggestive of radical-directed fragmentation processes. The hydrogen atom losses from the precursor ions upon UVPD are shown for a series of PCs in Figure S6. To further investigate the nature of the hydrogen atom loss product, UVPD-CID of *m/z* 759.57 for PC 16:0/18:1(9Z) was performed (Figure S7). UVPD was used to generate the hydrogen loss product (*m/z* 759.57) which was subsequently isolated and subjected to CID. While there are obvious differences in fragment ion abundances between the UVPD and UVPD-CID spectra (Figure S7a versus S7b), in general, many of the ions present in the UVPD spectrum are also present in the UVPD-CID spectrum. However, there exist fragment ions unique to UVPD, namely the product ion of *m/z* 622.45 which is one of the key

diagnostic fragment ions used to determine double bond position. In the UVPD-CID, there is an alternate product ion of *m/z* 620.43 which is 26 Da lower in mass, not 24 Da lower in mass, than the companion ion of *m/z* 646.45.

The production of diagnostic product ions that differ by 24 Da upon UVPD is consistent for a number of PCs containing acyl chains with a single unsaturation, and interestingly it is 2 Da less than the difference between allylic cleavages observed by Pham *et al.* for a radical-directed dissociation (RDD) process[35] and for the products in the UVPD-CID spectra (Figure S5). Beyond the presence of diagnostic C-C cleavage products in the spectra of PC 18:1(9Z)/18:1(9Z) and PC 18:1(6Z)/18:1(6Z), there are differences in the abundances of these ions for each of the two isomers (Figure 2b and 2d) suggesting that the specific double bond position influences the fragmentation processes.

To further probe the influence of specific structural features on the observed UVPD spectra, HCD and UVPD spectra for a series of PCs were compared. Figure 3 shows the UVPD spectra for PC 18:0/18:0, PC 18:0/18:1(9Z) and PC 18:0/18:2(9Z, 12Z); the only variable feature is the number of double bonds. Figure S8 shows the corresponding HCD mass spectra. The UVPD spectrum for PC 18:0/18:1(9Z) (Figure 3b), as expected, contains a diagnostic ion pair of *m/z* 650.47 and *m/z* 674.47. The UVPD spectrum for PC 18:0/18:2 (9Z, 12Z) (Figure 3c) contains two sets of diagnostic ions of *m/z* 650.47 and *m/z* 674.47, and *m/z* 690.50 and *m/z* 714.50, indicating that the positions of multiple unsaturations within an acyl chain can be localized. However, in contrast to UVPD spectra of PCs with a single unsaturation in an acyl chain, the UVPD spectrum for PC 18:0/18:2(9Z,12Z) contains additional ions of *m/z* 675.47, *m/z* 676.48, *m/z* 688.49 and *m/z* 689.50, shown in the inset of Figure 3c. These fragments appear to correspond to odd electron fragments originating from homolytic cleavage of carbon-carbon bonds (*m/z* 675.48 and *m/z* 689.50) or fragments derived from radical-directed processes (*m/z* 676.49 and *m/z* 688.49). The expanded regions of the UVPD mass spectra in Figure S6 confirm an increased abundance of the hydrogen atom loss product for PC 18:0/18:2(9Z,12Z) (see *m/z* 785.59) compared to isomeric PC 18:1(9Z)/18:1(9Z) and PC 18:1(6Z)/18:1(6Z). Figure 3d additionally shows how the number of double bonds influences HCD and UVPD efficiency as a function of precursor depletion. Precursor depletion is calculated as percentage of the surviving precursor ion after activation by HCD (NCE 25) or UVPD (10 pulses, 6 mJ). In general, the number of double bonds has little influence on the precursor depletion during HCD, whereas the number of double bonds significantly increases the depletion of the precursor upon UVPD. Increased precursor depletion may be related to an increase in UV photoabsorption cross-section and possibly more facile radical-mediated processes, both which scale with the number of double bonds.

For the acyl chain positional isomers PC 16:0/18:1(9Z) and PC 18:1(9Z)/16:0, HCD leads to preferential loss of acyl chains at the *sn-2* position as ketenes (Figure S9). This preferential loss results in the product ions of *m/z* 496.34 for PC 16:0/18:1(9Z) and *m/z* 522.36 for PC 18:1(9Z)/16:0. Although the abundances of acyl chain neutral loss ions may be skewed by the presence of contaminating isomers inherent to the sample, as has been previously reported,[15,41] the same overall trend holds between the positional isomers. In the UVPD spectra of the positional isomers, there appears to be preferential losses of the unsaturated acyl chains leading to more abundant ions at *m/z* 478.33 and *m/z* 496.34. Again, this

preference suggests that fragmentation is modulated by the presence of the double bond. However, there is no significant difference in the abundances of the fragment ions corresponding to cleavage of either carbon-carbon bond adjacent to the double bond. While it is difficult to determine whether specific fragments are generated via a charge-driven or charge-remote processes without performing experiments with specific deuterium-labeled PCs, it is likely that multiple fragmentation mechanisms contribute to the observed UVPD mass spectra. Moreover, the double bond positions, number of double bonds and acyl chain position may influence which fragmentation pathways are preferentially accessed.

While complete structural characterization of lipids is challenging, detection and differentiation of isomeric lipids in complex biological extracts is crucial for correlation of molecular structure with biological function. For analysis of PCs in biological samples, application of the developed UVPD method is well suited for a shotgun approach for two reasons: 1) as UVPD of PCs suffers from rather low fragmentation efficiency, a shotgun approach offers the ability to average multiple spectra for optimal signal to noise, and 2) while co-isolation and fragmentation of isobaric and isomeric lipids can create convoluted MS/MS spectra that can be challenging to interpret, the high resolution capabilities of the Orbitrap mass spectrometer enable identification of fragment ions with high confidence despite the presence of convoluting species. To demonstrate the UVPD strategy, a bovine liver extract was analyzed owing to its high PC content. Figure S10 shows the positive mode and negative mode shotgun MS1 mass spectra. The positive mode mass spectrum contains both protonated species and salt adducts for many phospholipids. High resolution and high mass accuracy allow empirical formulae to be determined from the MS1 spectra. For structural characterization of PC, ions throughout the mass spectrum were manually selected for subsequent MS/MS analysis. HCD was first performed to identify an ion as a PC species using the characteristic head group product ion of *m/z* 184.07. Negative mode HCD spectra of the formate adduct ($[M+COOH]^-$) was also collected to verify the acyl chain composition. If a precursor ion was identified as a PC, then the same precursor was subsequently isolated and subjected to UVPD in the positive mode. For example, HCD was performed on the ion of *m/z* 760.58 (observed in Figure 4a). The resulting HCD spectrum displayed an abundant fragment of *m/z* 184.07 indicative of a PC (Figure 4b). UVPD was then performed on the ion of *m/z* 760.58, and fragment ions with a difference of 24 Da were used to determine double bond positions (Figure 4c). Two sets of ions with a difference of 24 Da were observed in the UVPD spectrum: *m/z* 622.44 and 646.44 corresponding to PC 16:0_18:1(9Δ) and *m/z* 650.47 and 674.47 corresponding to PC 16:0_18:1(11Δ). HCD was performed on the formate-adducted species in negative mode (*m/z* 804.57, seen in Figure S10) to further confirm the acyl chain composition. Ions at *m/z* 255.23 and *m/z* 281.25 confirm palmitate (16 carbon chain) and oleate (18 carbon chain with 1 unsaturation) acyl chains. This strategy allows differentiation of isomeric PCs in biological samples. Table 1 contains a list of seventeen PCs identified in the bovine liver extract with localized double bonds and the corresponding diagnostics ions. Figures S11–20 show the corresponding positive mode HCD and UVPD spectra and negative mode HCD spectra for the identified PCs.

Substantial differences in the relative abundances of the diagnostic ions in the UVPD spectrum are apparent in Figure 4b. Comparison of the variations in relative abundances of

diagnostics ions between samples affords insight into changes in the isomer profiles. In fact, changes in the relative abundances of isomeric lipids have previously been correlated to disease states.[33] To assess the ability of the shotgun UVPD method to decipher changes in the relative isomer composition, mixtures containing various molar ratios of the isomers PC 18:1(6Z)/18:1(6Z) and PC 18:1(9Z)/18:1(9Z) (with a fixed total concentration of 10 μM) were analyzed (Figure S21, S22). UVPD mass spectra were collected, and the abundances of the pair of diagnostic ions for PC 18:1(6Z)/18:1(6Z) were used to calculate the percentage of ion current attributed to PC 18:1(6Z)/18:1(6Z) relative to PC 18:1(9Z)/18:1(9Z)). Figure 5 confirms there is a linear relationship in the percent abundance of diagnostic ions that correlates with the concentration of PC 18:1(6Z)/18:1(6Z), thus providing a means to evaluate the composition of mixtures.

Conclusion

Although collisional activation of phospholipids provides head group and acyl chain information, isobaric/isomeric structures resulting from variations in double-bond position and acyl chain position often go undetermined. The presented results confirm that 193 nm UVPD allows PC double bond positional isomers to be discerned. Comparison of the fragmentation patterns of a series of PCs gave insight into the underlying pathways promoted by UVPD. The series of collected spectra suggest that both the number of double bonds and their relative positions influence photoactivation and fragmentation. A shotgun method utilizing HCD and UVPD in conjunction with the high resolution capabilities of the Orbitrap mass analyzer affords the ability to analyze complex mixtures of phospholipids. From a bovine polar liver extract seventeen PCs were identified, all with double bonds localized. Additionally, preliminary quantitative studies indicate that relative changes in isomer composition can be detected in biological samples. We are currently extending the UVPD method to other subclasses of phospholipids to gain a more detailed global profile of the phospholipids present in biological samples. Despite the advantages of the developed strategy, it is currently not a high throughput method. While automated peak selection and acquisition of MS^2 spectra could easily be implemented into this method, identification of lipids from UVPD spectra remains a bioinformatics challenge. Most existing lipid identification software that use MS^2 spectra for identification cater to collision-based fragmentation methods and do not assign peaks originating from cleavage of C-C bonds. Thus, the development of more sophisticated lipid analysis software is essential. In addition, while shotgun spectra are inherently complex, shotgun UVPD spectra are more so, which poses challenges for spectra interpretation and identification of lower abundance species. Coupling of a gas-phase separation method, like differential mobility spectrometry, could allow for spectral simplification while still permitting analysis to be performed in a shotgun fashion.[16]

Supplementary Material

Refer to Web version on PubMed Central for supplementary material.

Acknowledgments

Funding from the NIH (R01 GM103655) and the Welch Foundation (F-1155) is gratefully acknowledged.

References

1. Brown SHJ, Mitchell TW, Oakley AJ, Pham HT, Blanksby SJ. J Am Soc Mass Spectrom. 2012; 23(9):1441–1449. [PubMed: 22669763]
2. Remaut, H., Fronzes, R., editors. Bacterial Membranes: Structural and Molecular Biology. Horizon Scientific Press; 2014.
3. Zhang YM, Rock CO. Nat Rev Microbiol. 2008; 6(3):222–233. [PubMed: 18264115]
4. Hussain NF, Siegel AP, Ge Y, Jordan R, Naumann CA. Biophys J. 2013; 104(10):2212–2221. [PubMed: 23708361]
5. van Meer G, Voelker DR, Feigenson GW. Nat Rev Mol Cell Biol. 2008; 9(2):112–124. [PubMed: 18216768]
6. Shevchenko A, Simons K. Nat Rev Mol Cell Biol. 2010; 11(8):593–598. [PubMed: 20606693]
7. Blanksby SJ, Mitchell TW. Annu Rev Anal Chem. 2010; 3(1):433–465.
8. Wenk MR. Nat Rev Drug Discov. 2005; 4(7):594–610. [PubMed: 16052242]
9. Janmey PA, Kinnunen PKJ. Trends Cell Biol. 2006; 16(10):538–546. [PubMed: 16962778]
10. Sandra K, Sandra P. Curr Opin Chem Biol. 2013; 17(5):847–853. [PubMed: 23830914]
11. Holthuis JCM, Levine TP. Nat Rev Mol Cell Biol. 2005; 6(3):209–220. [PubMed: 15738987]
12. Martinez-Seara H, Róg T, Pasenkiewicz-Gierula M, Vattulainen I, Karttunen M, Reigada R. Biophys J. 2008; 95(7):3295–3305. [PubMed: 18621818]
13. Brouwers JF. Biochim Biophys Acta Mol Cell Biol Lipids. 2011; 1811(11):763–775.
14. Damen CWN, Isaac G, Langridge J, Hankemeier T, Vreeken RJ. J Lipid Res. 2014; 55(8):1772–1783. [PubMed: 24891331]
15. Maccarone AT, Duldig J, Mitchell TW, Blanksby SJ, Duchoslav E, Campbell JL. J Lipid Res. 2014; 55(8):1668–1677. [PubMed: 24939921]
16. Lintonen TPI, Baker PRS, Suoniemi M, Ubhi BK, Koistinen KM, Duchoslav E, Campbell JL, Ekroos K. Anal Chem. 2014; 86(19):9662–9669. [PubMed: 25160652]
17. Pulfer M, Murphy RC. Mass Spectrom Rev. 2003; 22(5):332–364. [PubMed: 12949918]
18. Wenk MR. Cell. 2010; 143(6):888–895. [PubMed: 21145456]
19. Brügger B. Annu Rev Biochem. 2014; 83(1):79–98. [PubMed: 24606142]
20. Han X, Yang K, Gross RW. Mass Spectrom Rev. 2012; 31(1):134–178. [PubMed: 21755525]
21. Han X, Gross RW. Mass Spectrom Rev. 2005; 24(3):367–412. [PubMed: 15389848]
22. Schuhmann K, Almeida R, Baumert M, Herzog R, Bornstein SR, Shevchenko A. J Mass Spectrom. 2012; 47(1):96–104. [PubMed: 22282095]
23. Schuhmann K, Herzog R, Schwudke D, Metelmann-Strupat W, Bornstein SR, Shevchenko A. Anal Chem. 2011; 83(14):5480–5487. [PubMed: 21634439]
24. Hsu FF, Turk J. J Chromatogr B. 2009; 877(26):2673–2695.
25. Wasslen KV, Canez CR, Lee H, Manthorpe JM, Smith JC. Anal Chem. 2014; 86(19):9523–9532. [PubMed: 25208053]
26. Canez CR, Shields SWJ, Bugno M, Wasslen KV, Weinert HP, Willmore WG, Manthorpe JM, Smith JC. Anal Chem. 2016; 88(14):6996–7004. [PubMed: 27275841]
27. Stutzman JR, Blanksby SJ, McLuckey SA. Anal Chem. 2013; 85(7):3752–3757. [PubMed: 23469867]
28. Rojas-Betancourt S, Stutzman JR, Londry FA, Blanksby SJ, McLuckey SA. Anal Chem. 2015; 87(22):11255–11262. [PubMed: 26477819]
29. Ho YP, Huang PC, Deng KH. Rapid Commun Mass Spectrom. 2003; 17(2):114–121. [PubMed: 12512089]
30. Hsu FF, Turk J. J Am Soc Mass Spectrom. 2008; 19(11):1681–1691. [PubMed: 18771936]

31. Ma X, Xia Y. Angew Chem. 2014; 126(10):2630–2634.
32. Stinson CA, Xia Y. Analyst. 2016:3696–3704. [PubMed: 26892746]
33. Ma X, Chong L, Tian R, Shi R, Hu TY, Ouyang Z, Xia Y. Proc Natl Acad Sci. 2016; 113(10): 2573–2578. [PubMed: 26903636]
34. Yang K, Zhao Z, Gross RW, Han X. Anal Chem. 2011; 83(11):4243–4250. [PubMed: 21500847]
35. Pham HT, Ly T, Trevitt AJ, Mitchell TW, Blanksby SJ. Anal Chem. 2012; 84(17):7525–7532. [PubMed: 22881372]
36. Pham HT, Trevitt AJ, Mitchell TW, Blanksby SJ. Rapid Commun Mass Spectrom. 2013; 27(7): 805–815. [PubMed: 23495027]
37. Pham HT, Julian RR. Int J Mass Spectrom. 2015; 378:225–231.
38. Kozlowski R, Mitchell T, Blanksby S. Eur J Mass Spectrom. 2015; 21(3):191–200.
39. Brown SHJ, Mitchell TW, Blanksby SJ. Biochim Biophys Acta Mol Cell Biol Lipids. 2011; 1811(11):807–817.
40. Pham HT, Maccarone AT, Thomas MC, Campbell JL, Mitchell TW, Blanksby SJ. Analyst. 2014; 139(1):204–214. [PubMed: 24244938]
41. Campbell JL, Baba T. Anal Chem. 2015; 87(11):5837–5845. [PubMed: 25955306]
42. Deimler RE, Sander M, Jackson GP. Int J Mass Spectrom. 2015; 390:178–186. [PubMed: 26644782]
43. Li P, Hoffmann WD, Jackson GP. Int J Mass Spectrom. 2016; 403:1–7. [PubMed: 27547107]
44. Liang X, Liu J, LeBlanc Y, Covey T, Ptak AC, Brenna JT, McLuckey SA. J Am Soc Mass Spectrom. 2007; 18(10):1783–1788. [PubMed: 17719238]
45. Brodbelt JS. Chem Soc Rev. 2014; 43(8):2757–2783. [PubMed: 24481009]
46. Madsen JA, Cullen TW, Trent MS, Brodbelt JS. Anal Chem. 2011; 83(13):5107–5113. [PubMed: 21595441]
47. O'Brien JP, Brodbelt JS. Anal Chem. 2013; 85(21):10399–10407. [PubMed: 24083420]
48. O'Brien JP, Needham BD, Henderson JC, Nowicki EM, Trent MS, Brodbelt JS. Anal Chem. 2014; 86(4):2138–2145. [PubMed: 24446701]
49. O'Brien JP, Needham BD, Brown DB, Trent MS, Brodbelt JS. Chem Sci. 2014; 5(11):4291–4301. [PubMed: 25386333]
50. Hankins JV, Madsen JA, Giles DK, Brodbelt JS, Trent MS. Proc Natl Acad Sci. 2012; 109(22): 8722–8727. [PubMed: 22589301]
51. Shaw JB, Li W, Holden DD, Zhang Y, Griep-Raming J, Fellers RT, Early BP, Thomas PM, Kelleher L, Brodbelt JS. J Am Chem Soc. 2013; 135(34):12646–12651. [PubMed: 23697802]
52. Klein DR, Holden DD, Brodbelt JS. Anal Chem. 2016; 88(1):1044–1051. [PubMed: 26616388]
53. Liebisch G, Vizcaino JA, Köfeler H, Trötzmüller M, Griffiths WJ, Schmitz G, Spener F, Wakelam MJO. J Lipid Res. 2013; 54(6):1523–1530. [PubMed: 23549332]
54. Hsu, FFu, Turk, J. J Am Soc Mass Spectrom. 2003; 14(4):352–363. [PubMed: 12686482]

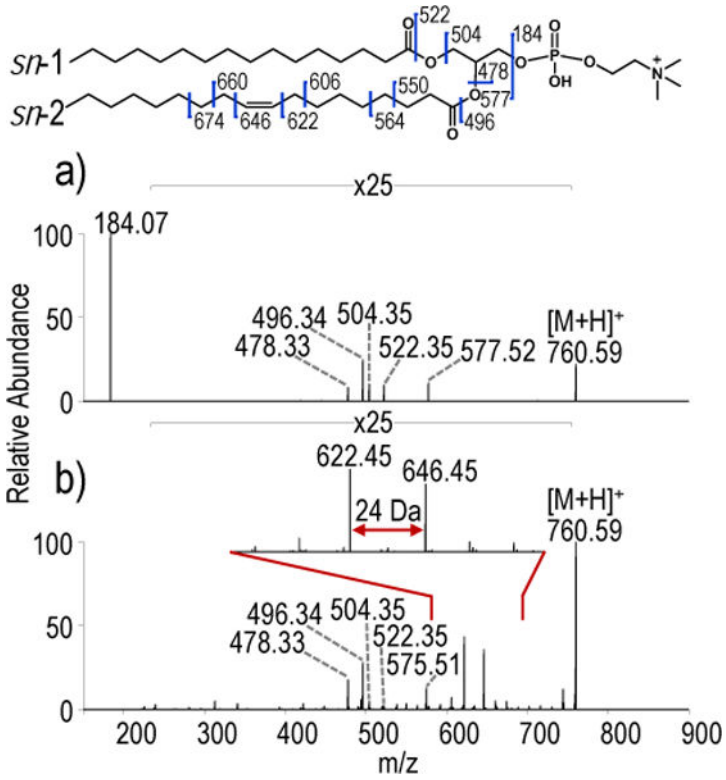

Figure 1.

a) HCD (NCE 25) and b) UVPD (10 pulses, 6 mJ) spectra of protonated PC 16:0/18:1(9Z) ($[M+H]^+$, *m/z* 760.58).

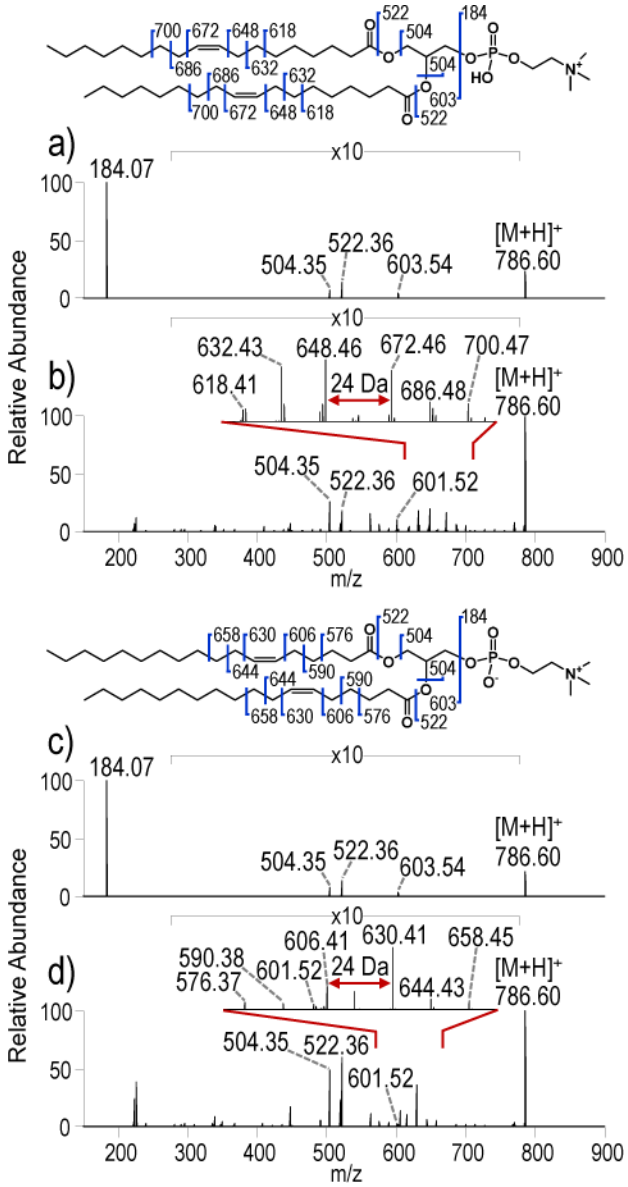

Figure 2.

a) HCD (NCE 25) and b) UVPD (10 pulses, 6 mJ) spectra of protonated PC 18:1(9Z)/18:1(9Z) ($[M+H]^+$, *m/z* 786.60). c) HCD (NCE 25) and UVPD (10 pulses, 6 mJ) spectra of protonated PC 18:1(6Z)/18:1(6Z) ($[M+H]^+$, *m/z* 786.60).

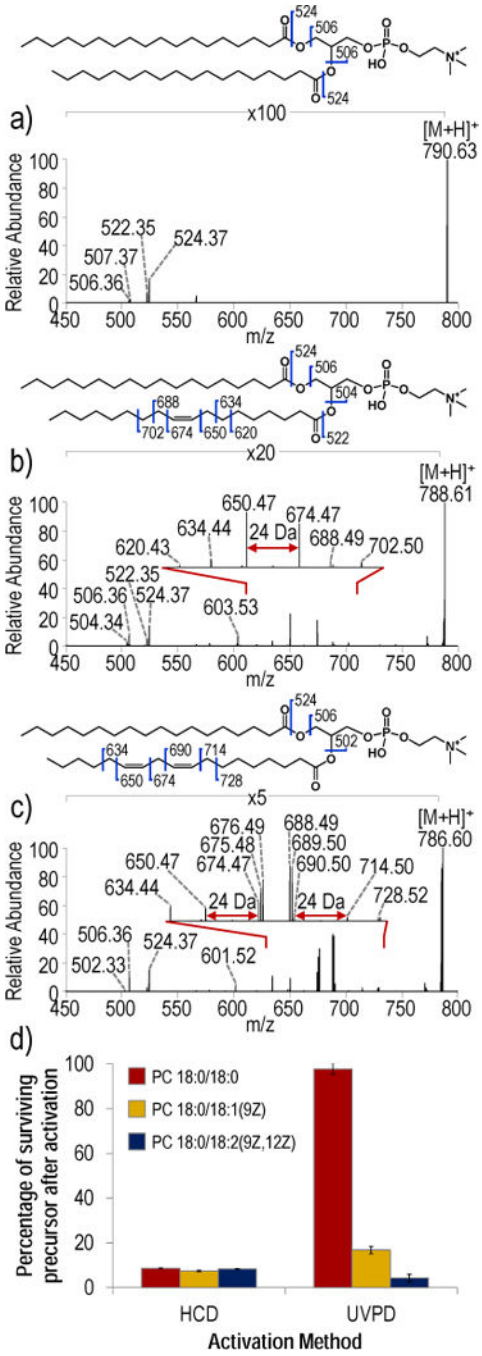

Figure 3.

UVPD spectra (10 pulses, 6 mJ) of a) PC 18:0/18:0 ($[M+H]^+$, *m/z* 790.63), b) PC 18:0/18:1(9Z) ($[M+H]^+$, *m/z* 788.61), and PC 18:0/18:2(9Z,12Z) ($[M+H]^+$, *m/z* 786.60). d) Bar graph comparing the impact of the number of double bonds on HCD and UVPD as a function of precursor depletion measured as the percentage of surviving precursor after activation.

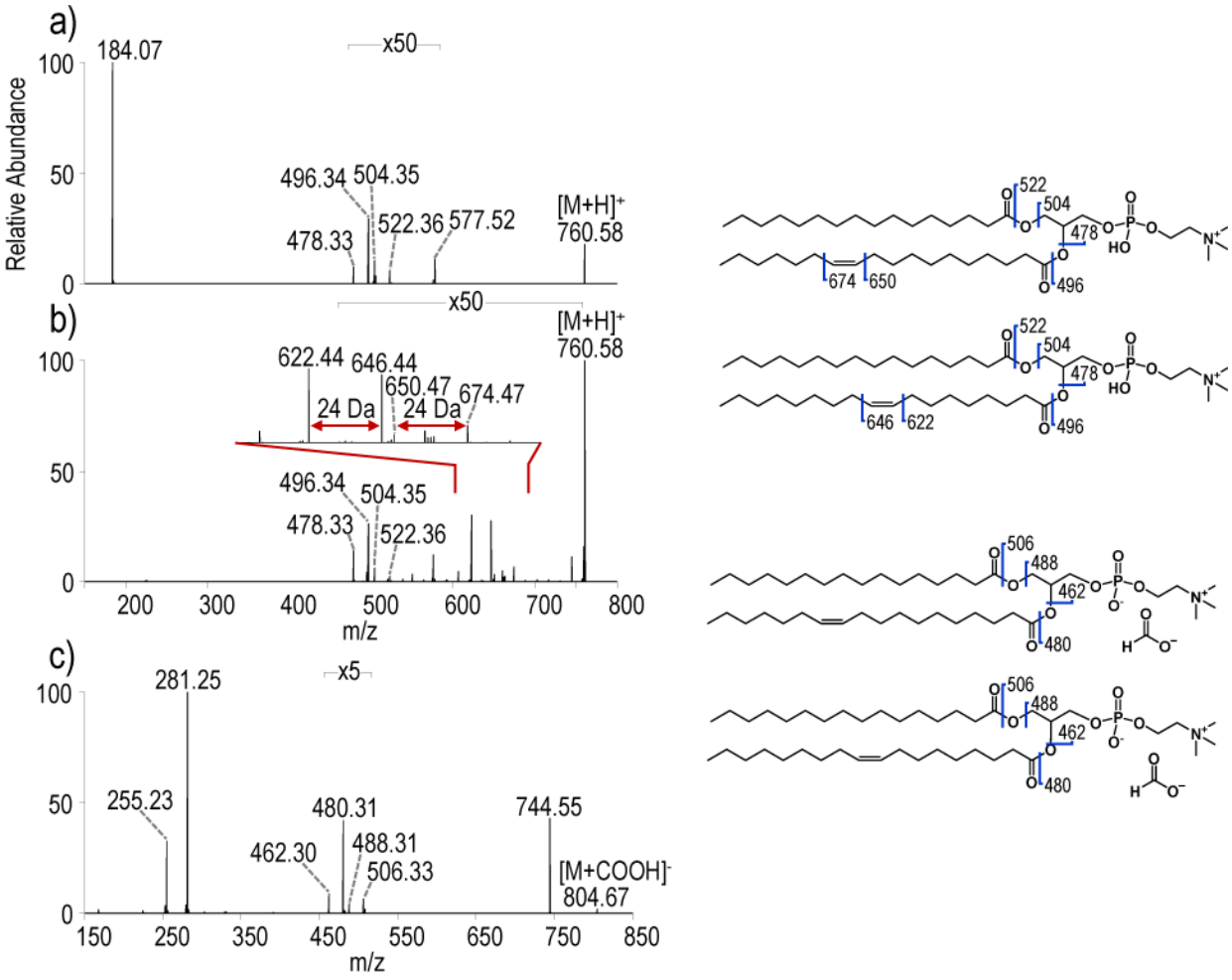

Figure 4.

Positive mode a) HCD (NCE 25) and b) UVPD spectra (10 pulses, 6 mJ) of m/z 760.58, ($[M+H]^+$) and c) negative mode HCD spectrum of *m/z* 804.67, ($[M+COOH]^-$).

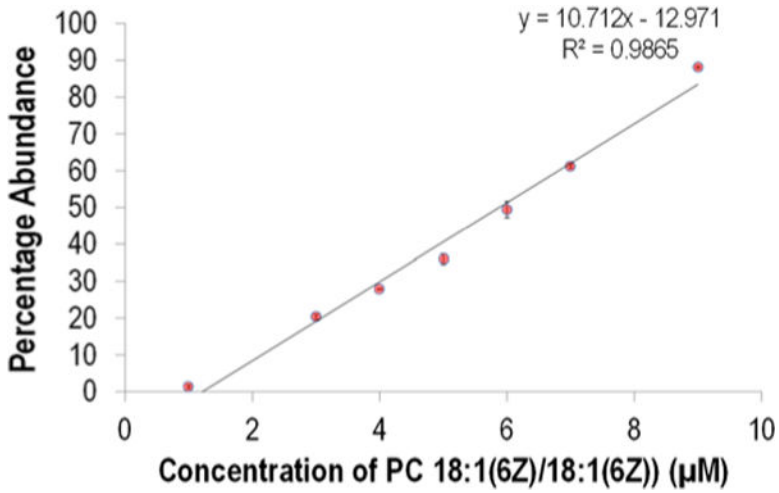

Figure 5.

Plot confirming the linear relationship between the concentration of PC 18:1(6Z)/18:1(6Z) (x-axis) and the percentage of the abundance that the diagnostic ions from PC 18:1(6Z)/18:1(6Z) (*m/z* 606 + *m/z* 630) comprise relative to the total abundance of all the diagnostic ions ion (*m/z* 606 + *m/z* 630 + *m/z* 648 + *m/z* 672) (y-axis). Mixtures containing various ratios of the isomers PC 18:1(6Z)/18:1(6Z) and PC 18:1(9Z)/18:1(9Z) (with a fixed total concentration of 10 μM) were analyzed.

Table 1

List of identified PCs from polar liver extract (positive and negative mode)

Identified unsaturated PCs	Precursor $[M+H]^+$ (*m/z*)	Diagnostic ions for double bond position (*m/z*)	Precursor $[M+CHOO]^-$ (*m/z*)	Acyl chain fragment ions (*m/z*)
PC 14:0_18:1 (9Δ)	732.55	594.41, 618.41	776.54	227.20, 281.25
PC 16:0_16:1 (9Δ)	732.55	622.44, 646.44	776.54	253.22, 255.23
PC 16:0_18:1 (9Δ)	760.58	622.44, 646.44	804.57	255.23, 281.25
PC 16:0_18:1 (11Δ)	760.58	674.47, 650.47	804.56	255.23, 281.25
PC 16:0_18:2 (9Δ,12Δ)	758.57	622.44, 646.44, 662.47, 686.47	802.56	255.23, 279.23
PC 16:0_20:3 (8Δ,11Δ,14Δ)	784.58	608.43, 632.43, 648.46, 672.46, 688.49	828.57	255.23, 305.23
PC 16:0_22:4(7Δ,10Δ,13Δ,16Δ)	810.60	594.41, 618.41, 634.33, 658.44, 698.47, 714.50	854.59	255.23, 331.26
PC 18:0_18:1 (9Δ)	788.61	650.47, 674.47	832.60	281.25, 283.25
PC 18:0_18:1 (11Δ)	788.61	678.50, 702.51	832.60	281.25, 283.25
PC 18:0_18:2 (9Δ,12Δ)	786.60	650.47, 674.47, 690.50, 714.51	830.59	279.23, 283.26
PC 18:0_18:3 (6Δ,9Δ,12Δ)	784.58	608.43, 632.43, 648.46, 672.46, 688.49	828.57	277.22, 283.26
PC 18:1(10Δ)_18:1 (10Δ)	786.60	662.47, 686.48	830.59	281.25
PC 18:1 (9Δ)_18:2 (9Δ,12Δ)	784.58	646.43, 670.43, 648.46, 672.46, 688.49	828.57	279.23, 281.25
PC 18:0_20:3(8Δ,11Δ,14Δ)	812.61	636.46, 660.46, 676.49, 700.49	856.60	283.26, 305.25
PC 18:0_20:4 (5Δ,8Δ,11Δ,14Δ)	810.60	594.41, 618.41, 634.33, 658.44, 698.47, 714.50	854.59	283.26, 303.23
PC 18:0_22:4 (7Δ,10Δ,13Δ,16Δ)	838.63	622.44, 646.44, 662.47, 686.47, 702.50, 726.51, 742.53	882.62	283.26, 331.26
PC 18:0_22:5 (7Δ,10Δ,13Δ,16Δ,19Δ)	836.61	622.44, 646.44, 662.47, 686.47, 726.50, 766.54	880.61	283.26, 329.25